JOURNAL OF MAGNETIC RESONANCE IMAGING 31:1185–1194 (2010)

Original Research

Accuracy and Repeatability of Fourier Velocity Encoded M-Mode and Two-Dimensional Cine Phase Contrast for Pulse Wave Velocity Measurement in the Descending Aorta

Valentina Taviani, MSc,[1,2]* Andrew J. Patterson, PhD,[1] Martin J. Graves, MSc,[1] Christopher J. Hardy, PhD,[3] Pauline Worters, PhD,[4] Michael P.F. Sutcliffe, PhD,[2] and Jonathan H. Gillard, MD[1]

Purpose: To assess the accuracy and repeatability of Fourier velocity encoded (FVE) M-mode and two-dimensional (2D) phase contrast with through-plane velocity encoding (2D-PC) for pulse wave velocity (PWV) evaluation in the descending aorta using five different analysis techniques.

Materials and Methods: Accuracy experiments were conducted on a tubular human-tissue-mimicking phantom integrated into a flow simulator. The theoretical PWV value was derived from the Moens-Korteweg equation after measurement of the tube elastic modulus by uniaxial tensile testing (PWV = 6.6 ± 0.7 m/s). Repeatability was assessed on 20 healthy volunteers undergoing three consecutive MR examinations.

Results: FVE M-mode PWV was more repeatable than 2D-PC PWV independently of the analysis technique used. The early systolic fit (ESF) method, followed by the maximum of the first derivative (1st der.) method, was the most accurate (PWV = 6.8 ± 0.4 m/s and PWV = 7.0 ± 0.6 m/s, respectively) and repeatable (inter-scan within-subject variation $\delta = 0.096$ and $\delta = 0.107$, respectively) for FVE M-mode. For 2D-PC, the 1st der. method performed best in terms of accuracy (PWV = 6.8 ± 1.1 m/s), whereas the ESF algorithm was the most repeatable ($\delta = 0.386$).

Conclusion: FVE M-mode allows rapid, accurate and repeatable central PWV evaluation when the ESF algorithm is used. 2D-PC requires long scan times and can provide accurate although much less repeatable PWV measurements when the 1st der. method is used.

Key Words: pulse wave velocity; Fourier velocity encoding; phase contrast; foot-finding algorithm
J. Magn. Reson. Imaging 2010;31:1185–1194.

REDUCED ARTERIAL COMPLIANCE has been shown to be related to age, hypertension, atherosclerosis, and coronary heart disease (1–3). In longitudinal studies, aortic stiffness has been found to independently predict coronary events and strokes after adjustment for traditional cardiovascular risk factors such as diabetes, positive smoking history, and LDL-cholesterol levels (4,5). Fast and reliable techniques for monitoring arterial stiffness are essential to assess the response to therapy in individuals with hypertension, heart failure, and other vascular diseases (6).

Pulse wave velocity (PWV), which is defined as the rate of propagation of the pressure or flow wave travelling along the artery, can be used as a measure of arterial stiffness. PWV is related to the Young's modulus E and the distensibility coefficient D through the following equations:

$$PWV = \sqrt{\frac{Eh}{2\rho r}} \quad [1]$$

$$PWV = \sqrt{\frac{1}{\rho D}} \quad [2]$$

where h is the vessel wall thickness, ρ is the blood density and r is the vessel radius at end diastole. Equation [1], known as the Moens-Korteweg equation, assumes that the vessel wall thickness is small

[1]Department of Radiology, Cambridge University Hospitals NHS Foundation Trust, Hills Road, Cambridge, United Kingdom.
[2]Department of Engineering, Cambridge University, Trumpington Street, Cambridge, United Kingdom.
[3]GE Global Research, One Research Circle, Niskayuna, New York, New York, USA.
[4]Department of Radiology, Stanford University, Lucas Center, Stanford, California, USA.
Contract grant sponsor: National Institute of Health Research, Biomedical Research Centre, EPSRC DTA, Cambridge European Trust and Royal Society.
*Address reprint requests to: V.T., Department of Radiology, University of Cambridge, Addenbrooke's Hospital, Box 218, Cambridge CB2 0QQ, UK. E-mail: vt232@cam.ac.uk
Received August 25, 2009; Accepted February 2, 2010.
DOI 10.1002/jmri.22143
Published online in Wiley InterScience (www.interscience.wiley.com).

compared with the diameter, and that the fluid within the vessel is inviscid and incompressible.

PWV is usually estimated by dividing the distance between two anatomical locations by the time lag between the pressure or flow waveforms recorded at the two different locations. Doppler ultrasound and applanation tonometry have been widely used to estimate carotid–femoral PWV as a surrogate of aortic PWV (7,8). However, both these techniques are operator-dependent and because the distance between the two measurement sites is estimated on the basis of surface anatomy, PWV values can be easily overestimated, particularly in obese subjects (9).

MR imaging can be used to assess central aortic stiffness noninvasively with minimal errors from inaccurate distance measurements. Several MR-based methods have been proposed, including multisite 2D phase contrast with through-plane velocity encoding (10,11), 2D phase contrast performed in an oblique–sagittal plane covering the aorta with in-plane velocity encoding (12,13) and flow sensitive 4D MRI (14). Other MR-based techniques have been proposed that allow PWV measurements very rapidly and with improved temporal resolution (15–17). Two-dimensional phase contrast with through-plane velocity encoding performed at two or more locations along the aorta is the most commonly reported approach in clinical studies, despite the long acquisition time necessary to achieve sufficient temporal resolution. In some cases, application of the flow-area method (18) allows PWV estimation from a single phase contrast slice. Repeatability of 2D phase-contrast-derived PWV values in the proximal pulmonary arteries was assessed using a transit time algorithm by Bradlow et al (19). On a smaller cohort of healthy volunteers, Rogers et al found no statistically significant differences in PWV values from 2D phase contrast when two consecutive acquisitions based on different localizers were performed, and after removing and repositioning the subject in the scanner (20).

Fourier velocity encoded (FVE) MR M-mode is an interleaved one dimensional technique which has been shown to be a fast method for determining PWV in the descending aorta (21). Accuracy of MR M-mode with standard phase contrast velocity encoding for PWV evaluation (15) was demonstrated against intravascular pressure measurements conducted on a flow phantom by Bolster et al (22). Although feasibility of FVE M-mode has already been demonstrated in vivo (21), its accuracy and repeatability have not been reported.

In this study FVE M-mode and multisite 2D phase contrast with through-plane velocity encoding were compared in terms of the accuracy and repeatability of the derived PWV values. Five different analysis methods for PWV evaluation previously reported in the literature were applied to FVE M-mode and phase contrast images and compared. Repeatability of FVE M-mode and 2D phase contrast for each of the analysis methods considered was assessed on a cohort of 20 healthy volunteers undergoing three MR examinations each (*Repeatability Experiment*). The accuracy of the different methods was tested in a separate experiment conducted using a human-tissue-mimicking phantom integrated into a flow simulator, with the theoretical PWV value derived from Eq. [1] after uniaxial tensile tests performed on the flow phantom (*Accuracy Experiment*).

MATERIALS AND METHODS

Repeatability Experiment

Twenty healthy volunteers (11 men, 9 women) aged 24–57 years (mean age, 37 years) gave written informed consent to take part in the study. Local ethics committee approval was obtained. Each subject underwent three MR examinations on two separate visits. During the first visit, after the complete MR protocol had been performed, each subject was removed from the scanner room and, after repositioning of the subject and coil into the magnet bore, the same MR protocol was repeated. During the second visit, 1 week apart from the first one, each subject underwent a single MR examination during which the same protocol was repeated.

Accuracy Experiment

A custom-made polyvinyl alcohol cryogel (PVA-C) tube (inner diameter = 8.5 ± 0.3 mm, outer diameter = 10.68 ± 0.03 mm, length = 30 cm, T_1 = 1600 ms, T_2 = 65 ms) was used to model the compliant vessel (23). The tube was integrated into an existing physiological flow simulator as described by Wong et al (24). The two ends of the PVA-C tube were clamped to the inlet and outlet of a Perspex box, which was filled with water to produce MR signal outside the vessel model and avoid susceptibility artifacts caused by interfaces with air. To reduce waveform distortion and suppress unwanted dynamic effects, the box was connected to the pump and the reservoir by means of rigid polybutylene (PBT) tubes. A computer-controlled motor-driven pump (G4-KCT-KKA, ECO Gearchem, West Sussex, UK) was used to produce physiologically realistic flow waveforms. An aortic type waveform with peak and average flow rates of 30 mL/s and 15 mL/s, respectively, was used in all the experiments at a frequency of 60 beats/min to give velocities and deformations comparable to those found in vivo. Blood-mimicking fluid (T_1 = 850 ms, T_2 = 170 ms, ρ = 1020 kg/m^3) was used as the working fluid (Shelley Medical Imaging Technologies, Ontario, Canada).

The theoretical PWV value was derived from the Moens-Korteweg equation [1] after measurement of the elastic modulus of the tube by uniaxial tensile testing. A reference value derived directly from the mechanical behavior of the phantom and not based on the analysis of recorded waveforms, allowed assessment of the performance of the different algorithms without introducing any bias.

Uniaxial tensile tests were conducted on specimens extracted from the PVA-C tube to measure the elastic modulus E. Each specimen, consisting of an axial 40 mm long section of the tube, was clamped to the grips of a dedicated uniaxial tensile testing machine (Instron 5544, High Wycombe, Bucks, UK) and pulled

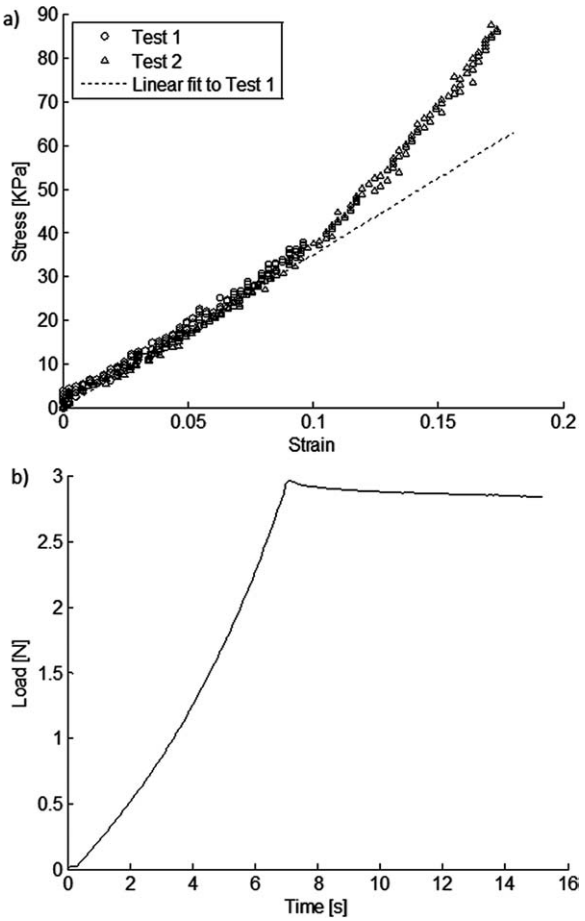

Figure 1. a: Stress-strain curve for the PVA-C phantom obtained by uniaxial tensile testing. Test 1: a 40-mm-long axial section of the tube is pulled along its axis at an extension rate of 1 mm/s (maximum strain = 18%). Test 2: a 10-mm-long axial section of the tube is cut open and the resulting strip is pulled along its major dimension (extension rate = 1 mm/s, maximum strain = 10%). **b:** A 40-mm-long axial section of the tube is pulled along its axis at an extension rate of 5 mm/s (maximum strain = 18%): the load vs. time curve is recorded to investigate eventual viscoelastic effects.

along the axis to a maximum extension of 35 mm at an extension rate of 1–5 mm/s. The applied force was recorded as a function of the specimen's extension and translated into the corresponding stress-strain curve after the specimen's dimensions were carefully measured (Fig. 1a, Test 1). Tests performed on smaller specimens cut out of the tube wall showed that the material was isotropic (Fig. 1a, Test 2). No significant viscoelastic effects were observed (Fig. 1b). The stress-strain curve for the PVA-C phantom showed nonlinear behavior as previously reported by Chu and Rutt (25). Because the maximum strain induced in the tube wall by the pulsatile flow waveform did not exceed 10%, linear regression of the stress-strain curve up to a 10% strain yielded an elastic modulus E = 0.34 ± 0.02 MPa (mean ± standard deviation refers to nine tests performed on two specimens) and, using Eq. [1], a PWV value of 6.6 ± 0.7 m/s.

Image Acquisition

Images were acquired on a 1.5 Tesla (T) whole-body imaging system (Signa HDx, GE Healthcare, Waukesha, WI). FVE M-mode was previously reported by Hardy et al (21). The pulse sequence consisted of a cylindrical excitation pulse (pulse width = 3.6 ms), followed by a bipolar velocity-encoding gradient (length of the bipolar pulse = 5.3 ms) and a readout gradient applied along the axis of the cylinder or "pencil" (Fig. 2). The sequence was gated to either a simulated or actual cardiac R-wave and executed 32 times per heart cycle (repetition time [TR] = 14 ms) with the bipolar gradient amplitude stepped to a new value on each new trigger. To increase the effective temporal resolution to 3.5 ms, four interleaves of the data were acquired, with the ECG trigger delay incremented by 3.5 ms each time, resulting in 128 time frames covering the first 450 ms of the cardiac cycle. Thirty-two velocity-encoding steps were used, yielding a true velocity resolution of 9.4 cm/s, which resulted in aliasing of velocities greater than 150 cm/s. A 24-cm readout field of view (FOV) (matrix size = 256 × 32), flip angle of 20° and a 2 cm diameter cylindrical excitation pulse were prescribed. Cylindrical excitation was achieved through an 8-cycle spiral trajectory (26) which resulted in an inner aliasing ring diameter of 28.5 cm. Off-resonance effects on the excitation profile, which can result in a broadening of the profile toward the extremities, were found to be negligible over the 24 cm FOV used in this study.

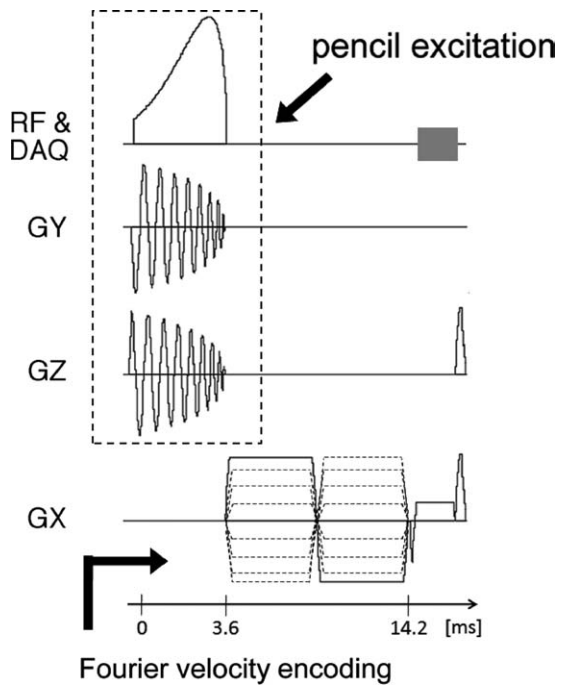

Figure 2. ECG-gated FVE M-mode pulse sequence comprises 2D pencil excitation pulse followed by stepped bipolar velocity encoding gradient and readout gradient oriented along the pencil axis. Two-dimensional Fourier transformation of the data results in a plot of velocity distribution versus position along the pencil.

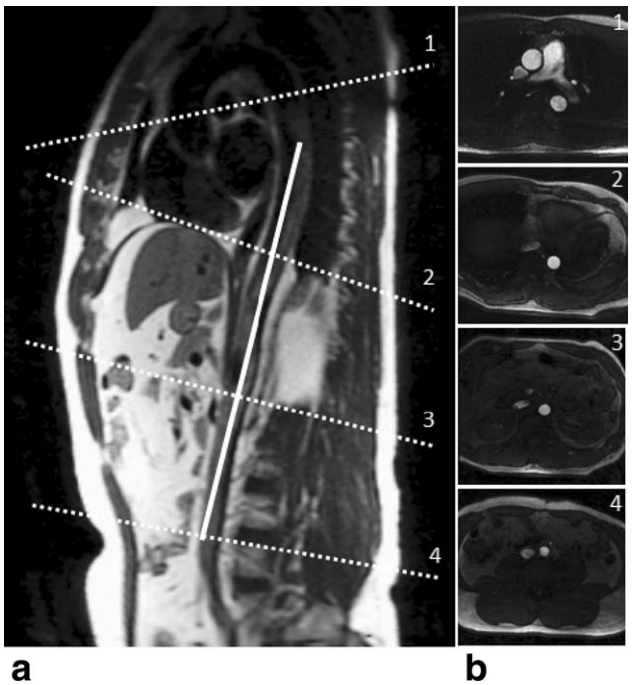

Figure 3. a: Oblique sagittal scout image from a healthy volunteer. Solid line indicates position of pencil for FVE M-mode; dashed lines indicate position of planes prescribed for 2D phase contrast with through-plane velocity encoding. **b:** Phase contrast magnitude images across the arch (1), at the level of the diaphragm (2), 3 cm above the aortic bifurcation (4), and midway (3) between locations (2) and (4).

Repeatability Experiment

Volunteers were scanned using an eight-channel phased-array surface coil. An oblique-sagittal fast spin-echo (FSE) with double inversion recovery blood suppression covering the length of the aorta was used as a scout image for prescribing the FVE M-mode sequence. Figure 3a shows the FSE scout with the white solid line denoting the prescription of the pencil excitation (the line's length denoting the FOV). Two-dimensional ECG-gated cine phase contrast with through-plane velocity encoding was prescribed at four locations along the aorta. Oblique transverse images perpendicular to the aorta were acquired: (1) at the level of the pulmonary trunk through the ascending and proximal descending aorta; (2) at the level of the diaphragm; (3) midway between location 2 and a location 3 cm proximal to the aortic bifurcation; and (4) 3 cm above the aortic bifurcation (Fig. 3).

The following imaging parameters were used in the phase contrast acquisition: TR = 6.7 ms, echo time (TE) = 3.2 ms, flip angle = 30°, FOV = 28 cm, slice thickness = 5 mm, VENC = 150 cm/s, signal averages = 2, views per segment = 1. The true temporal resolution was 2×TR. One hundred phases per R-R interval were retrospectively reconstructed.

Accuracy Experiment

For the phantom experiments, a 5-inch receive-only surface coil was placed directly on top of the water-filled Perspex box. All the sequences were triggered using simulated R-R waveforms produced by the flow simulator. FVE M-mode was graphically prescribed on a three-plane localizer with the pencil aligned along the length of the PVA-C tube. Two-dimensional cine phase contrast with through-plane velocity encoding was performed at three axial locations 6 cm apart.

The following imaging parameters were used for the phase contrast acquisition: TR = 7.6 ms, TE = 3.6 ms, field of view (FOV) = 14 cm; all other parameters were set as for the repeatability experiment.

Image Analysis

FVE M-mode image analysis was performed using a graphical user interface (GUI) developed in-house using Matlab version 7.5.0 (The Mathworks, Inc., Natick, MA). Figure 4a shows 6 of the 128 FVE M-mode velocity images acquired on a healthy volunteer who took part in the study. Each image corresponds to a specific temporal phase. The bright horizontal line in each frame represents static tissue within the excited pencil. Vertical displacements relative to each line are proportional to velocity at that cardiac phase. To track the propagation of the flow waveform along the vessel more easily, images were reformatted with the horizontal axis representing time and the vertical axis representing velocity (27) (Fig. 4b). Because velocity measurements were limited to the first half of the R-R interval, plug flow was observed for most of the acquired cardiac phases. In the presence of plug flow, the cross-sectional mode, mean and peak velocities are very similar, with the mode of the velocity spectrum represented by the locus of maximum-intensity pixels located above the static-tissue signal component. An automatic line detector was used to extract the mode velocity pattern (henceforth referred to as velocity profile) as a function of time from each of the obtained time-velocity images. For each pixel along the horizontal axis, i.e., for each temporal phase, the maximum pixel-intensity along the corresponding velocity axis was found. A threshold (2–3 pixels) was interactively set by the user for each data set to exclude the contribution of static tissue. In some subjects the time-velocity images were not visually discernible over the entire FOV. To have enough signal in all the time-velocity frames so that the velocity profile could be accurately identified, the length of the pencil to be considered for the analysis was chosen by the user through the GUI. In all subjects the length considered for the analysis was at least two thirds of the FOV used for FVE M-mode. The velocity profiles extracted from the time-velocity images at different positions along the vessel were visualized as a velocity surface, each point of which represented velocity at a given time and position (12,13). Bilinear interpolation and the gradient-based regularization technique implemented in the Matlab function *gridfit* (28) were used to smooth the obtained velocity surface. Visual comparison of the 3D surface generated by *gridfit* and the original data points excluded large-scale variations from being introduced into the velocity profile during the smoothing process.

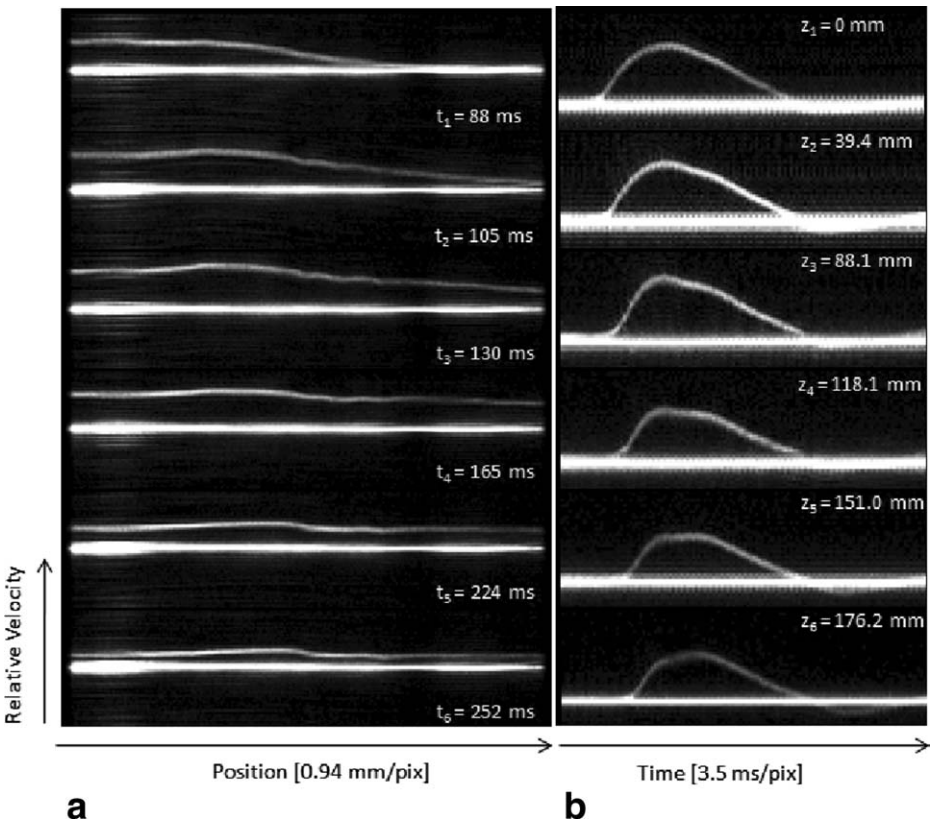

Figure 4. a: Six of the 128 FVE M-mode images each representing a different cardiac phase. The bright horizontal line in each frame represents static tissue within the pencil. Vertical displacements relative to each line represent blood velocity along the pencil at that cardiac phase. **b:** Six of 256 FVE M-mode images reformatted to visualize pulse wave propagation along the vessel. Each frame represents velocity (vertical axis) versus time (horizontal axis) at different positions along the aorta (z_1: most proximal; z_6: most distal). Plug flow was observed in most cardiac phases, because only the first 450 ms of the R-R interval was imaged.

Five different algorithms previously published in the literature were implemented to compute the PWV from the 3D velocity surface: (i) maximum of first derivative (1st der.) (29,30); (ii) maximum of second derivative (2nd der.) (31); (iii) early systolic fit (ESF) (21,32); (iv) cross-correlation (Xcorr.) (12); and (v) velocity correlation (Vcorr.) (33). The first four algorithms were transit-time methods; hence, PWV was computed by linear regression of the foot of the wave at each position along the vessel as a function of the corresponding location along the aorta. The statistical rigor of the fits was ensured by the large number of points (150–250) involved in the fitting process. Standard errors over the three MR examinations for FVE M-mode derived PWVs were 0.001 ± 0.0006, 0.0016 ± 0.0035, 0.0153 ± 0.0109, and 0.0009 ± 0.0009 when the 1st der., 2nd der., Xcorr., and ESF methods, respectively, were used (values reported as mean ± standard deviation; units: pixels along the vessel/pixels along temporal direction).

For the 1st der. method, the foot of the wave was defined as the point corresponding to the maximum of the first partial derivative of velocity with respect to time. Similarly, for the 2nd der. method the foot of the wave was defined as the point corresponding to the maximum of the second temporal derivative of velocity. For the 1st der. and 2nd der. methods, the original data points extracted from the time-velocity images were not interpolated and the smoothing parameter was chosen within a range of values for which PWV variation, as a function of the amount of smoothing introduced in the data, was found to be minimal.

In the ESF method, the foot of the wave was found at the intersection of a line fitted to the upslope portion of the velocity waveform (between 20% and 40% of the peak velocity) and the zero-velocity baseline. Interpolation was not used and data smoothing was kept to a minimum.

The Xcorr. method was implemented as described by Fielden et al (12), except that cross-correlation was limited to the first half of the velocity profile. The number of points in the time direction was increased 10-fold using bilinear interpolation with the smoothing parameter kept to a minimum. Waveforms at each location along the vessel were compared with the waveform corresponding to one end of the pencil using a cross-correlation function. The foot of the wave at each location was defined as the time shift between the current and reference waveform for which the cross-correlation function was maximum.

In the Vcorr. method, the second partial derivative of velocity with respect to time and position were numerically evaluated using a central finite difference formula on a 3-point stencil. The original data points derived

Table 1
Repeatability Experiment*

	FVE M-mode				2D CINE phase contrast			
	PWV(±SD) (m/s)	Intra-day COV (%)	Inter-day COV (%)	δ (m^2/s^2)	PWV (±SD) (m/s)	Intra-day COV (%)	Inter-day COV (%)	δ (m^2/s^2)
1st der.	4.7 (±0.75)	1.00	1.31	0.107	4.9 (±0.78)	2.74	2.01	0.431
2nd der.	4.5 (±0.71)	1.47	2.15	0.196	5.2 (±0.96)	2.59	2.43	0.690
Xcorr.	5.2 (±0.86)	1.48	1.54	0.143	5.7 (±1.36)	3.56	2.71	1.412
Vcorr.	5.0 (±0.68)	1.43	1.78	0.152	4.3 (±0.83)	3.48	3.36	0.543
ESF	4.9 (±0.67)	0.70	1.62	0.096	4.7 (±0.70)	2.82	2.15	0.386

*Group mean and standard deviation PWV (±SD), intra-day and inter-day coefficients of variation (COV) expressed as a percentage relative to the group mean, and inter-scan within-subject variation (δ) as determined by a one-way analysis of variance random-effect model. FVE = Fourier velocity encoded.

from the time-velocity images were not interpolated and the smoothing parameter was chosen as for the 1st der. and 2nd der. algorithms. For the computation of the second temporal derivative, adjacent points in the time direction were used. Numerical evaluation of the second spatial derivative was difficult because noise was of the same order of magnitude. To improve accuracy in the computation of the spatial derivative, the pencil's length (l = FOV) was divided into three segments and only the central one was considered for the analysis. The derivative at a given location z and time t within the central segment was then computed using velocity data at ($z-l/3$,t) and ($z+l/3$,t). The second temporal derivative was plotted as a function of the second spatial derivative at each location along the vessel and a line was fitted to each of these plots. PWV was computed as the square root of the mean slope.

It should be noted that, unlike the original implementations of the Xcorr. and Vcorr. methods, where the mean cross-sectional velocity at any given spatial location and temporal phase was used, the velocity derived from the FVE M-mode data represents the mode of the velocity spectrum at a given spatial location and temporal phase. Because plug flow was observed for most of the acquired cardiac phases and in the presence of plug flow the mode and mean velocity are very similar, this difference is expected to have minimal impact on the derived PWV values.

Velocity waveforms were extracted from phase contrast images using commercial software (CV Flow v.3.1, Medis, Leiden, The Netherlands). Savitzky-Golay filtering was performed before the PWV analysis. For the phase contrast slice at the level of the pulmonary trunk, only the velocity profile within the descending aorta was considered for PWV evaluation. The same methods described for FVE M-mode were applied to phase-contrast-derived velocity waveforms. In the Xcorr. method, cross-correlation was performed on the entire velocity profile, as in the original implementation by Fielden et al (12). For the Vcorr. method, adjacent points in both the spatial and temporal direction were used for the numerical evaluation of the derivatives over the entire velocity profile.

Statistical Analysis

A one-way analysis-of-variance random linear mixed-effects model was performed to quantify different sources of variation. Quan and Shih previously applied this approach to assess reproducibility by quantifying the within-subject variation and between-subject variability separately (34). This study has applied this approach and uses the computational methodology described by Faraway to apply a one-way analysis-of-variance random-effect model to calculate the within-subject variance between scans 1, 2, and 3 (35). The population's mean intra- and inter-day coefficients of variation are also reported. Thus, repeatability for each of the five image analysis techniques as applied to FVE M-mode and phase-contrast-derived PWV measurements is reported using within-subject variation and the population-mean intra- and inter-day coefficient of variation.

All the analysis was performed using the statistical programming language R version 2.5.1 (The R Foundation for Statistical Computing, Vienna, Austria). The within-subject variation was quantified using the linear and nonlinear mixed-effects package (version 3.1-88).

RESULTS

Repeatability Experiment

Results for the repeatability experiments are summarized in Table 1. One subject was excluded from the study due to the poor quality of the FVE M-mode images, making analysis impossible. The inter-scan within-subject variation (δ) was lower for FVE M-mode than for phase contrast independently of the analysis technique used, meaning a better repeatability of FVE M-mode over phase contrast. For FVE M-mode the intra-day repeatability was better than the inter-day repeatability irrespective of the analysis method used. For phase contrast instead the inter-day repeatability was always marginally better than the intra-day repeatability. For both MR techniques, the ESF method was found to be the most repeatable (FVE M-mode: $\delta = 0.096$; phase contrast: $\delta = 0.386$) followed by the 1st der. method (FVE M-mode: $\delta = 0.107$; phase contrast: $\delta = 0.431$). The least repeatable was Xcorr. ($\delta = 1.412$) for phase contrast and 2nd der. ($\delta = 0.196$) for FVE M-mode.

Accuracy Experiment

FVE M-mode and phase contrast-derived PWV values as obtained using the 1st der., 2nd der., ESF, Xcorr.,

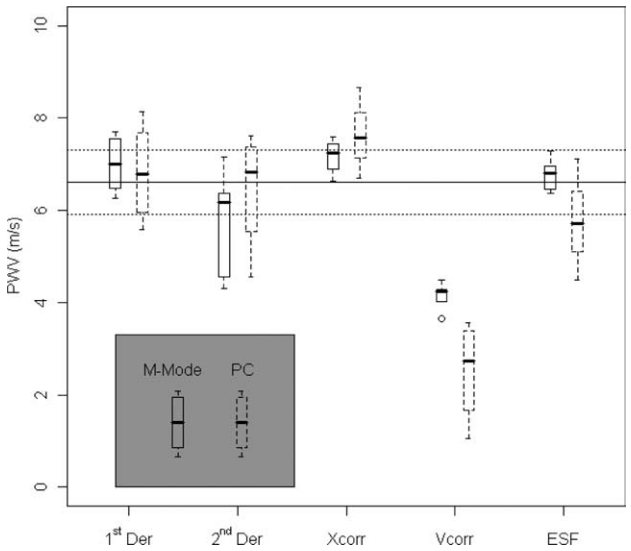

Figure 5. Accuracy experiment: PWV measurements conducted on a compliant tube segment integrated into a flow simulator. PWV values as determined using FVE M-mode and 2D phase contrast with through-plane velocity encoding and the 1st der., 2nd der., ESF, Xcorr., and Vcorr. methods for image analysis. The techniques are plotted beside the defined reference PWV ± 1 standard deviation.

and Vcorr. methods are shown in Figure 5 against the theoretical PWV value (6.6 ± 0.7 m/s) derived from the Moens-Korteweg equation. ESF applied to FVE M-mode was found to be the most accurate method (6.8 ± 0.4 m/s). For phase contrast, the 1st der. method proved to be the most accurate (6.8 ± 1.1 m/s). The same method was also found to perform well with FVE M-mode (7.0 ± 0.6 m/s). The 2nd derivative method used with phase contrast gave better agreement with the reference PWV than when applied to FVE M-mode images (phase contrast: 6.8 ± 1.6 m/s; FVE M-mode: 5.7 ± 1.2 m/s). While the Xcorr. method was found to overestimate slightly the PWV when applied to both phase contrast and FVE M-mode (phase contrast: 7.7 ± 1.4 m/s; FVE M-mode: 7.1 ± 0.4 m/s), Vcorr. underestimated the PWV with both imaging techniques (phase contrast: 2.5 ± 1.1 m/s; FVE M-mode: 4.1 ± 0.3 m/s). For all analysis methods, ranges were greater for phase contrast than for FVE M-mode.

DISCUSSION

Five different methods previously published in the literature to derive PWV values from velocity data were applied to FVE M-mode and 2D phase contrast images and were compared in terms of accuracy and repeatability. FVE M-mode proved to be more repeatable than phase contrast independently of the analysis technique used to extract the PWV. For both imaging techniques the ESF method was found to be the most repeatable followed by the 1st der. method. These same two algorithms were also the most accurate for M-mode while for phase contrast the two most accurate algorithms were the 1st der. and the 2nd der.

Phase contrast has been widely used to evaluate PWV in the aorta (10,11) and some studies have been performed to assess its repeatability (19,20). FVE M-mode, in contrast, has only been demonstrated to be feasible in vivo (21) with no study reporting on accuracy and repeatability. One of the main advantages of FVE M-mode over phase contrast is the substantial reduction in acquisition time. An FVE M-mode acquisition with 32 velocity encoding steps and 4 interleaves as performed in this study took 128 heartbeats to complete, i.e., approximately 2 min for a heart rate of 60 beats/min. For the same heart rate, 2D phase contrast with through-plane velocity encoding performed at a given location along the aorta took more than twice as long as an M-mode acquisition, and because at least two slices were needed to obtain the PWV, the minimum scan time for a PWV examination would have been over 8 min.

PWV values derived from FVE M-mode were found to be more repeatable than those extracted from phase contrast independently of the analysis technique used. The effective temporal resolution was 3.5 ms and 13.4 ms for FVE M-mode and phase contrast, respectively; therefore, the intrinsic uncertainty in PWV was higher for phase contrast irrespective of the analysis method used. In addition, with phase contrast, two or more velocity images need to be acquired. In the limiting case of only two slice locations and when a transit time algorithm is used to estimate the PWV, errors in the position of the foot of the wave directly translate into PWV errors. PWV estimation is more robust when several velocity profiles at different locations along the vessel are analyzed and PWV is computed as the inverse of the slope of the best-fit line for the plot representing the position of the foot of the wave as a function of the corresponding location along the vessel. FVE M-mode yielded a series of time-velocity profiles with a spatial resolution along the length of the pencil of less than 1 mm in approximately 2 min. For phase contrast, the imaging time was proportional to the number of acquired slices, so that increasing the number of velocity images quickly led to prohibitively long scan times. In this study, four phase-contrast velocity images at four different locations along the aorta were acquired with an average total scan time of approximately 16 min. Because PWV was ultimately determined with a best-fit calculation for all the analysis techniques considered, FVE M-mode-derived values, based on average on more than 170 data points, were less sensitive to local errors in the identification of the foot of the wave and hence more repeatable than the corresponding phase contrast values, obtained by best-fitting to only four points.

Some studies have reported on 2D phase contrast with in-plane velocity encoding performed in an oblique-sagittal plane containing the aorta for a more accurate central PWV evaluation (12,13). Although the results reported in (12) were in good agreement with the PWV values obtained using 2D phase contrast with through-plane velocity encoding performed in the

ascending and lower abdominal aorta, this method relies heavily on the imaging plane being precisely prescribed through the vessel centerline. The cylindrical excitation used in M-mode also relies upon identification of the vessel centerline for prescription; however, mispositioning of the pencil does not lead to substantial errors in the velocity images as in the case of in-plane velocity-encoded phase contrast, where the maximum velocity can be missed if the imaging plane does not contain the vessel centerline.

Despite being relatively insensitive to prescription errors, the M-mode pulse sequence is limited to straight and relatively large diameter vessel segments, like the aorta and the common carotid artery (27). While the aorta is a large vessel throughout its length, it can be tortuous, so that M-mode prescription over long segments of vessel can occasionally be difficult and eventually result in poor quality data.

FVE M-mode data quality was determined in part by the height of the FVE velocity waveforms, which was inversely related to the VENC. Setting a low VENC increases the velocity resolution and should therefore facilitate detection of the foot of the wave. However, high velocity-resolution images were often characterized by lower signal intensity, which sometimes made image segmentation uncertain. As a result, the VENC value was empirically determined to be low enough to yield a reasonable velocity resolution but not so low as to penalize the quality of the velocity spectra excessively.

For FVE M-mode the ESF method proved to be the most repeatable and accurate technique, followed by the 1st der. method. Hardy et al used an ESF method to extract the PWV from FVE M-mode images (21). Although our implementation of the ESF algorithm was very similar, following the propagation of the flow wave on the time-velocity images (instead of the position-velocity images) as suggested in (27), made the foot detection process more robust to image noise and reduced segmentation errors. Inter- and intra-observer variabilities ($r = 0.94$ and $r = 0.95$) for the ESF method applied to phase contrast images with through-plane velocity encoding were recently reported by Ibrahim et al who also confirmed good repeatability between different scans (36).

The ESF method proved to be the most repeatable also for phase contrast, followed again by the 1st der. method. Butlin et al assessed the repeatability of seven different transit time algorithms applied to phase contrast images and found that the intersecting tangents method was the most repeatable (37). According to this method, the foot of the wave is found at the intersection between two lines fitting the systolic upslope and late diastolic part of the velocity profile respectively. Because in M-mode imaging the diastolic flow signal is confounded with static-tissue signal, we decided not to consider this method.

The most accurate analysis technique for phase contrast was the 1st der. method followed by the 2nd der. method, although the latter did not prove to be accurate when applied to FVE M-mode and had a low repeatability for both MR techniques. The 2nd der. method was found to be very sensitive to filtering as already pointed out by Hermeling et al (31). The better performance in terms of accuracy when applied to phase contrast might be a consequence of the Savitzky-Golay filter's ability to preserve subtle features of the velocity profile which are otherwise flattened by the gradient-based smoothing technique used for FVE M-mode images.

The Vcorr. method performed worst in terms of accuracy. As already pointed out in (33) in relation to phase contrast, the Vcorr. method is very sensitive to the length of the segment considered for PWV evaluation with relative errors up to 68% for a distance of 4 cm between the phase contrast slices. For phase contrast, the separation between the imaging planes was limited to 6 cm due to the physical length of the phantom, whereas for FVE M-mode, the use of a 5-inch coil to maximize the image quality meant the available length for PWV evaluation was only 3 cm. In both cases, the reduced length of the segments used for PWV measurement led to substantially underestimated values with respect to the reference PWV value when using the Vcorr. method.

Similarly, the poor repeatability of the Xcorr. method when applied to phase contrast images was mainly because only three points were fitted to obtain the PWV. In the original study by Fielden et al (12), in-plane velocity encoding was used, and thus a relatively high number of points were generated. The FVE M-mode velocity data share this advantage, and in this case, repeatability of the Xcorr. method was found to be substantially higher than for multislice phase-contrast with through-plane velocity encoding.

Catheter pressure measurements are a widely accepted gold standard for in vitro studies of PWV. However, because one of the objectives of this work was to assess the best analysis technique for both FVE M-mode and phase contrast images, our "gold standard" was defined as the PWV value derived from the Moens-Korteweg equation after measurement of the phantom elastic modulus by uniaxial tensile testing. Using catheter pressure measurements as the gold standard would have involved taking a given foot-finding algorithm as a reference for all the other analysis methods, introducing a bias in the accuracy results.

The Moens-Korteweg equation is based on the assumptions that the tube is infinitely long and thin-walled and that the fluid within is inviscid and incompressible. While incompressibility of the blood-mimicking fluid is a good assumption, adherence of the Moens-Korteweg equation to measured or computationally predicted values in cases when the other assumptions are not met has been previously investigated. Fukui et al carried out a series of numerical simulations with fluid-structure interaction on a straight vessel model of limited length and finite wall thickness with blood flow and demonstrated that the Moens-Korteweg equation is in good agreement with their computational model for PWVs up to 10 m/s irrespective of the tube wall thickness (38). Callaghan et al showed that in the canine common carotid artery, which is dimensionally similar to the phantom used for our experiments, PWV values as predicted by

the Moens-Korteweg equation after measurement of the vessel elastic modulus agreed well with values derived from intravascular pressure measurements over a relatively wide range of pressures (39). In the descending aorta, Duprez et al confirmed adherence of the Moens-Korteweg equation to MR-derived PWV values in a middle-aged cohort of healthy volunteers (40).

A limitation of this study is the limited age range considered for the in vivo repeatability study. Because PWV has been demonstrated to increase with age, a wider age range would allow testing of the different techniques also in cases of higher PWV values, which, intuitively, are more difficult to evaluate. Otherwise, our results are in agreement with previously reported values. For example, Mohiaddin et al studied 20 healthy volunteers aged 16–59 years and found a mean PWV value of 5.6 ± 1.4 m/s (32). Rogers et al reported 6.7 ± 2.5 m/s for an under-55 cohort of 9 healthy volunteers (20).

In conclusion, we have shown that FVE M-mode allows accurate and repeatable estimates of PWV in the descending aorta when images are analyzed using the ESF or 1st der. method. Two-dimensional phase contrast with through-plane velocity encoding performed at four locations along the aorta in conjunction with the 1st der. method provides accurate although much less repeatable PWV measurements. The limited scan time required for FVE M-mode (2 min.) makes it a valuable tool to perform PWV examinations within the framework of clinical MR protocols.

ACKNOWLEDGMENT

The authors thank Dr. I.B. Wilkinson and Dr. C.M. McEniery for useful discussion and ongoing collaboration and Ilse Joubert (MR radiographer) for performing the volunteer study.

REFERENCES

1. Izzo JL Jr, Mitchell GF. Aging and arterial structure-function relations. Adv Cardiol 2007;44:19–34.
2. McEniery CM, Cockcroft JR. Does arterial stiffness predict atherosclerotic coronary events? Adv Cardiol 2007;44:160–172.
3. McEniery CM, Wilkinson IB, Avolio AP. Age, hypertension and arterial function. Clin Exp Pharmacol Physiol 2007;34:665–671.
4. Laurent S, Boutouyrie P. Arterial stiffness: a new surrogate end point for cardiovascular disease? J Nephrol 2007;20(Suppl 12): S45–S50.
5. Laurent S, Cockcroft J, Van Bortel L, et al. Expert consensus document on arterial stiffness: methodological issues and clinical applications. Eur Heart J 2006;27:2588–2605.
6. Laurent S, Kingwell B, Bank A, Weber M, Struijker-Boudier H. Clinical applications of arterial stiffness: therapeutics and pharmacology. Am J Hypertens 2002;15:453–458.
7. Boutouyrie P, Vermersch S, Laurent S, Briet M. Cardiovascular risk assessment through target organ damage: role of carotid to femoral pulse wave velocity. Clin Exp Pharmacol Physiol 2008; 35:530–533.
8. Podolec P, Kopec G, Podolec J, et al. Aortic pulse wave velocity and carotid-femoral pulse wave velocity: similarities and discrepancies. Hypertens Res 2007;30:1151–1158.
9. Karamanoglu M. Errors in estimating propagation distances in pulse wave velocity. Hypertension 2003;41:e8; author's reply, e8.
10. Grotenhuis HB, Ottenkamp J, Fontein D, et al. Aortic elasticity and left ventricular function after arterial switch operation: MR imaging–initial experience. Radiology 2008;249:801–809.
11. van der Meer RW, Diamant M, Westenberg JJ, et al. Magnetic resonance assessment of aortic pulse wave velocity, aortic distensibility, and cardiac function in uncomplicated type 2 diabetes mellitus. J Cardiovasc Magn Reson 2007;9:645–651.
12. Fielden SW, Fornwalt BK, Jerosch-Herold M, Eisner RL, Stillman AE, Oshinski JN. A new method for the determination of aortic pulse wave velocity using cross-correlation on 2D PCMR velocity data. J Magn Reson Imaging 2008;27:1382–1387.
13. Yu HY, Peng HH, Wang JL, Wen CY, Tseng WY. Quantification of the pulse wave velocity of the descending aorta using axial velocity profiles from phase-contrast magnetic resonance imaging. Magn Reson Med 2006;56:876–883.
14. Markl M, Wallis W, Brendecke S, et al. Optimized estimation of global and regional aortic pulse wave velocity. In: Proceedings of the 17th Annual Meeting of ISMRM, Honolulu, 2009.
15. Hardy CJ, Bolster BD, McVeigh ER, Adams WJ, Zerhouni EA. A one-dimensional velocity technique for NMR measurement of aortic distensibility. Magn Reson Med 1994;31:513–520.
16. Macgowan CK, Henkelman RM, Wood ML. Pulse-wave velocity measured in one heartbeat using MR tagging. Magn Reson Med 2002;48:115–121.
17. Shao X, Fei DY, Kraft KA. Rapid measurement of pulse wave velocity via multisite flow displacement. Magn Reson Med 2004;52: 1351–1357.
18. Vulliemoz S, Stergiopulos N, Meuli R. Estimation of local aortic elastic properties with MRI. Magn Reson Med 2002;47:649–654.
19. Bradlow WM, Gatehouse PD, Hughes RL, et al. Assessing normal pulse wave velocity in the proximal pulmonary arteries using transit time: a feasibility, repeatability, and observer reproducibility study by cardiovascular magnetic resonance. J Magn Reson Imaging 2007;25:974–981.
20. Rogers WJ, Hu YL, Coast D, et al. Age-associated changes in regional aortic pulse wave velocity. J Am Coll Cardiol 2001;38: 1123–1129.
21. Hardy CJ, Bolster BD Jr, McVeigh ER, Iben IE, Zerhouni EA. Pencil excitation with interleaved Fourier velocity encoding: NMR measurement of aortic distensibility. Magn Reson Med 1996;35: 814–819.
22. Bolster BD Jr, Atalar E, Hardy CJ, McVeigh ER. Accuracy of arterial pulse-wave velocity measurement using MR. J Magn Reson Imaging 1998;8:878–888.
23. Surry KJ, Austin HJ, Fenster A, Peters TM. Poly(vinyl alcohol) cryogel phantoms for use in ultrasound and MR imaging. Phys Med Biol 2004;49:5529–5546.
24. Wong P, Graves MJ, Lomas DJ. Integrated physiological flow simulator and pulse sequence monitoring system for MRI. Med Biol Eng Comput 2008;46:399–406.
25. Chu KC, Rutt BK. Polyvinyl alcohol cryogel: an ideal phantom material for MR studies of arterial flow and elasticity. Magn Reson Med 1997;37:314–319.
26. Hardy CJ, Bottomley PA. 31P spectroscopic localization using pinwheel NMR excitation pulses. Magn Reson Med 1991;17: 315–327.
27. Hardy CJ, Marinelli L, Blezek DJ, Darrow RD. MRI determination of pulse wave velocity in the carotid arteries. In: Proceedings of the 16th Annual Meeting of ISMRM, Toronto, 2008.
28. D'Errico J. Surface fitting using gridfit. Matlab Central 2006. Available at: http://www.mathworks.com/matlabcentral/fileexchange/8998. Accessed October 2008.
29. Millasseau SC, Stewart AD, Patel SJ, Redwood SR, Chowienczyk PJ. Evaluation of carotid-femoral pulse wave velocity: influence of timing algorithm and heart rate. Hypertension 2005;45:222–226.
30. Asmar R, Benetos A, Topouchian J, et al. Assessment of arterial distensibility by automatic pulse wave velocity measurement. Validation and clinical application studies. Hypertension 1995;26: 485–490.
31. Hermeling E, Reesink KD, Reneman RS, Hoeks AP. Measurement of local pulse wave velocity: effects of signal processing on precision. Ultrasound Med Biol 2007;33:774–781.
32. Mohiaddin RH, Firmin DN, Longmore DB. Age-related changes of human aortic flow wave velocity measured noninvasively by magnetic resonance imaging. J Appl Physiol 1993;74:492–497.
33. Urchuk SN, Plewes DB. A velocity correlation method for measuring vascular compliance using MR imaging. J Magn Reson Imaging 1995;5:628–634.

34. Quan H, Shih WJ. Assessing reproducibility by the within-subject coefficient of variation with random effects models. Biometrics 1996;52:1195–1203.
35. Faraway JJ. Extending the linear model with R: generalized linear, mixed effects and nonparametric regression models. London: Chapman & Hall/CRC; 2006. ix, 301 p.
36. Ibrahim EH, Johnson KR, White RD. Different techniques for measuring aortic pulse wave velocity using magnetic resonance imaging. In: Proceedings of the 17th Annual Meeting of ISMRM, Honolulu, 2009.
37. Butlin M, Hickson S, Graves MJ, McEniery CM, Avolio AP, Wilkinson I. Determining pulse wave velocity using MRI: a comparison and repeatability of results using seven transit time algorithms. Artery Res 2008;2:99.
38. Fukui T, Imai Y, Tsubota K, Ishikawa T, Wada S, Yamaguchi T. A fluid-solid interaction study of the pulse wave velocity in uniform arteries. In: Proceedings of the Final Symposium of the Tohoku University 21st Century Center of Excellence Program, Sendai, Japan, 2007.
39. Callaghan FJ, Geddes LA, Babbs CF, Bourland JD. Relationship between pulse-wave velocity and arterial elasticity. Med Biol Eng Comput 1986;24:248–254.
40. Duprez DA, Swingen C, Sih R, Lefebvre T, Kaiser DR, Jerosch-Herold M. Heterogeneous remodelling of the ascending and descending aorta with age. J Hum Hypertens 2007;21:689–691.